

## Alginate-chitosan/carbon nanotubes nanocomposites: an efficient alternative for Co(II) ions removal

Azeem Bibi<sup>a</sup>, Sadiq-ur-Rehman<sup>a,\*</sup>, Muhammad Zaheer<sup>b</sup>, Tasleem Akhtar<sup>c</sup>

<sup>a</sup>Department of Chemistry, University of Azad Jammu and Kashmir, Muzaffarabad, Pakistan, Tel. +92 3018086819; emails: srkhattak@gmail.com (Sadiq-ur-Rehman), azeembibi786@gmail.com (A. Bibi)

<sup>b</sup>Department of Chemistry and Chemical Engineering, SBA School of Science and Engineering, Lahore University of Management Sciences (LUMS), Lahore 54792, Pakistan, email: muhammad.zaheer@lums.edu.pk

<sup>c</sup>Department of Zoology, University of Azad Jammu and Kashmir, Muzaffarabad, Pakistan, email: seemeawan88@gmail.com

Received 13 April 2021; Accepted 18 July 2021

### ABSTRACT

Alginate-based sorbents were successfully synthesized for Co(II) ions removal from an aqueous solution. Novel sorbents were prepared by entrapping COOH-MWCNTs (multi-walled carbon nanotubes) in the Algi+Chito matrix by solution casting method under ultrasonic waves without any crosslinker. Physico-chemical studies were carried out by Fourier transform infrared spectroscopy, scanning electron microscopy, X-ray diffraction, transmission electron microscopy, thermogravimetric analysis/differential scanning calorimetry, and Brunauer–Emmett–Teller analysis. Various factors such as contact time, concentration, temperature, pH, and co-existence of foreign ions were explicated. The adsorption capacity of 381, 380, and 383 mg g<sup>-1</sup> was achieved at 400 ppm, 3 h, and 25°C. Kinetics followed was pseudo-second-order and equilibrium adsorption data were fitted to the Langmuir linear and Freundlich nonlinear isotherm models, proved by  $\chi^2$  values. Adsorption was favorable with  $\Delta G^\circ$  values, -515.92, -511.15, and -530.10 kJ mol<sup>-1</sup> for nanocomposites. Sorbents also showed affinity to Co(II) ions along with other foreign ions. Sorbents were regenerated (six times) into the initial form for the next removal operation.

*Keywords:* Alginate-chitosan; Sorbents; Nanocomposites; Adsorption study; Films; Co<sup>2+</sup> ions

### 1. Introduction

Water pollution is a global issue and is caused by rapid industrialization, urbanization, and environmental changes. These sources contribute to unwanted anthropogenic pollutants in the ecosystems [1]. Metals are placed at the top of pollutants due to inclusion in water from acid mines drainages, industrial activities, and are considered major threats to the ecosystem. In industry, power plants release a dump of heavy and radioactive metals per year that can persist for decades [2]. Among these metals, cobalt is considered a wide-spreading pollutant and is used in superalloys, recording media, industry, catalysts, and porcelain materials [2].

Although the metabolic process in human beings needs a small amount of cobalt, its higher amount is toxic and causes lung effects, nausea, vision problems, heart problems, thyroid damage, sterility, and permanent disability [3]. Carcinogenicity-International Agency for Research on Cancer (IARC) and the Federal Republic of Germany has listed the cobalt ions in group 2B, which are possibly carcinogenic [4]. To prevent such acute toxicity, there is a dire need to discover new and efficient water-purifying methods. Several methods such as chemical precipitation [5], electrochemical deposition [6], ion exchange [7], and membrane separation [8] were traditionally applied to remove pollutants in past. However, these methods were complicated,

\* Corresponding author.

instrument-intensive, selective, expensive, and showed a low detection limit, which prohibits their application for on-site analysis. Therefore, in developing countries, there was a demand for economical, convenient, and simple processes.

Adsorption method based on physico-chemical interaction is one of the preferred methods used for preventing water pollution caused by heavy metal ions [9]. The high demand for the adsorption technique is due to relatively low cost, simple design, easy operation, smaller harmful by-products, wide availability of adsorbents, and easy retrieval [10]. Various adsorbents like clays, synthetic polymers, and solid industrial wastes were used previously but they had low adsorption capacity and were difficult to recycle [11]. Recently, it is believed that natural polymers act as good adsorbents with the best separation power, easy availability, low toxicity, and tunable porosity [12]. Additionally, the desired properties in natural polymers can produce by surface activation, grafting, or blending with appropriate compounds [13].

Sodium alginate is a natural porous polymer and is investigated in adsorption studies due to its biodegradability, biocompatibility, renewability, non-toxicity, and encapsulating nature [14]. It is comparatively cheaper obtained from brown algae, having a variable amount of D-mannuronic acid (M) and L-guluronic acid (G) units [15,16]. The polymeric backbone of alginate is flourished with hydroxyl and carboxyl groups which are considered very reactive to monovalent and polyvalent cations [2]. The film-forming, crosslinking and complex-forming properties of alginate are due to these surface functional groups that find wide applications in the fields of pharmaceuticals, cosmetics, food, agriculture, chemical engineering, and paper industry [17]. Similarly, chitosan is another naturally existing cationic polymer obtained from the crabs, prawns, and fungi. The D-glucosamine and N-acetyl-D-glucosamine units of the chitosan chains contain various  $\text{NH}_3$  groups. The reactive, flexible, and film-forming nature of chitosan is due to the  $\text{NH}_3$  functional group and have been exploited in metal ion sorption, catalysis, and drug delivery [18]. However, the pristine form of these polymers (alginate and chitosan) is flimsy and flexible with poor elasticity and mechanical strength [2,19]. So, it is the utmost need to find any reinforcing material, which can improve the strength of naturally existing polymers while maintaining the adsorbing property.

Introducing nanoparticles into polymeric materials can increase the chemical, mechanical, electrical, and surface properties. Alginate-CNTs (carbon nanotubes) nanocomposites attracted great attention because of their multi-dimensional properties such as high surface area, lighter weight, high aspect ratio, and eco-friendly nature [2,20–22]. However, the previously mentioned nanomaterials have some limitations like water solubility, fragility, bearing plentiful chemicals, and toxic nature. Therefore, in the current study, the strength of natural polymers (alginate) is improved by a greener approach, in which natural cationic polymer (chitosan) and COOH-MWCNTs are blended with alginate gel without any crosslinker under ultrasonic waves. A polyelectrolytic complex forms due to the reaction of the COOH group of alginates with the  $\text{NH}_3$  group of chitosan at room temperature [23]. In the alginate-chitosan complex, stability and mechanical strength are improved

by incorporating COOH-MWCNTs. Thus, the prepared materials are expected to be more porous, water-insoluble, cheap, natural, and renewable sorbents that will not only purify the contaminated water but will also solve the handling and disposal problem to a great extent.

To the best of our knowledge, no literature provides any proper information about the adsorption of Co(II) ions from the aqueous solution on alginate-chitosan/CNTs sorbents so far. Synthesized materials were characterized physico-chemically by Fourier transform infrared spectroscopy (FTIR), scanning electron microscopy (SEM), transmission electron microscopy (TEM), X-ray diffraction (XRD), thermogravimetric analysis/differential scanning calorimetry (TGA/DSC), and Brunauer–Emmett–Teller (BET) analysis. Co(II) ions were selected as a model pollutant to evaluate the adsorption capacity of synthesized films. The effect of various parameters like adsorbent dose, pH, temperature, and contact time was investigated in the Batch adsorption test. Linear and nonlinear kinetic isotherm and thermodynamic models were applied to experimental data to study the adsorption of target pollutants. Interference of various external metal ions in the adsorption capacity of Co(II) ions and recycling application of the synthesized sorbents have also been explained.

## 2. Experimental

### 2.1. Materials and methods

Sodium alginate (from brown algae, purity: 98%, CAS number: 9005-38-3, molecular weight: 120,000–190,000  $\text{g mol}^{-1}$ ), M/G ratio: 1.56, chitosan (purity: 99%,  $\geq 75\%$  deacetylated, CAS number: 9012-76-4, molecular weight: 20,000  $\text{g mol}^{-1}$ ), acetic acid, dimethylformamide, potassium chloride, bismuth chloride, calcium chloride, cobalt chloride ( $\text{CoCl}_2 \cdot 6\text{H}_2\text{O}$ ) and ferric chloride ( $\text{FeCl}_3 \cdot 6\text{H}_2\text{O}$ ) were purchased from Sigma-Aldrich (UK) and used without further purification. Functionalized multi-walled carbon nanotubes (COOH-MWCNTs) were kindly provided by the National Center for Physics (NCP), Pakistan. Deionized water was used throughout the procedure.

### 2.2. Preparation of nanocomposite films

Alginate-chitosan/COOH-MWCNTs nanocomposites were prepared by solution mixing method under ultrasonic waves (bath sonicator: Elmasonic S 30 (H), 50–60 H). Briefly, nanofillers (COOH-MWCNTs) were dispersed in an aqueous solution (20 mL) containing 0.1 g of surfactants (SDS and CTAB) by sonicating for 2 h at 40°C. The aqueous solution of sodium alginate was prepared by stirring 0.9 g of alginate powder in 40 mL of deionized water at 40°C for 3 h. Chitosan (0.18 g) was separately dissolved in 2% (w/v, 75 mL) of acetic acid solution at 40°C on continuous stirring for 3 h. Alginate-chitosan/COOH-MWCNTs nanocomposites (Cs90 (having SDS surfactant), Cc90 (having CTAB surfactant)) were formulated by adding alginate solution (2 mL, 0.045 g), chitosan solution (75 mL, 0.18 g), and surfactant-dispersed COOH-MWCNTs (2 mL, 0.1 g) in a conical flask. This blended mixture was sonicated for 3 h to form a homogeneous mixture at 40°C. Nanocomposite CD90 was prepared by a similar method except COOH-MWCNTs

were dispersed in 20 mL of DMF in place of an aqueous solution having surfactant. A homogeneous solution of nanocomposites was put in Petri plates and dried at room temperature. After drying in a dust-free environment for 2–3 weeks, the films of nanocomposites (0.121 mm) were obtained. Algi (0.05 mm) and Algi+Chito films (0.120 mm) were separately prepared by drying the dissolved solutions of pristine alginate and alginate-chitosan without nanofillers and surfactants. Finally, the obtained films were washed with ethanol and kept in an oven (for 5 h) at 40°C for complete dehydration. The dried films were sealed in polyethylene bags for further use.

### 2.3. Characterization techniques

Various instrumental techniques were applied to visualize the physico-chemical properties of synthesized materials. The surface morphology of nanocomposites was identified by using a scanning electron microscope (JOEL JSM-6510LV, Japan, 20 kV) and transmission electron microscope (JEOL JEM 1200 EXII) working at a voltage of 20.0 and 100.0 kV, respectively. Surface area and pore size were determined by BET (Quantachrome NOVA 2200e, USA) technique with 0.045 g of the sample at 273 K. Thermal behavior of synthesized films was checked by heating an adequate quantity of sample in the range of 0°C–700°C in thermal analyzer (TA SDT Q600). The shape, geometry, and pattern of arrangement in polymeric chains were determined by the XRD technique using a JDX-3532 diffractometer working at the voltage of 20–40 kV. The X-rays used were of 1.5418 Å to diffract the materials with a scanning range of 0°–160°. The nature of bonding and different functional groups present in nanocomposites was determined by FTIR spectroscopy (PerkinElmer Spectrum 100 Series Spectrometer, Korea).

### 2.4. Measurement of swelling capacity

In the continuation of this study, nanocomposites were also analyzed in swelling capabilities on immersing the films (14 mg) in 100 mL of distilled water, saline solutions (0.15 M, KCl, BiCl<sub>3</sub>, CaCl<sub>2</sub>, and FeCl<sub>3</sub> solution), and in the solution having variable pH (2–13) [24]. Swelling capacity was calculated by using Eq. (1) [25].

$$\text{Swelling} \left( \frac{\text{g}}{\text{g}} \right) = \frac{(W_s - W_d)}{W_d} \quad (1)$$

where  $W_s$  and  $W_d$  are 'swollen' and 'dry' weights of films at time 't', respectively.

### 2.5. Batch adsorption studies

For adsorption studies, a stock solution (1,000 mg L<sup>-1</sup>) of hexahydrated cobalt chloride was prepared by dissolving 1 g of salt in distilled water (1 L) at room temperature. For the isothermal adsorption experiment, a weighed portion (0.02 g) of each material was immersed in 20 mL of metal ions solution (5–700 ppm), stirred continuously on the hot plate at 200 rpm for 24 h. To separate the solid from liquid the sample was filtered off and unadsorbed Co<sup>2+</sup> ions in the filtrate were measured by UV-Vis spectrophotometer

(UV-1601 Shimadzu, Korea). The amount of adsorbed metal ions (mg g<sup>-1</sup>) on the surface of prepared nanocomposites was determined by using the following expressions [12,26].

$$q_e = \frac{(C_o - C_t)V}{W} \quad (2)$$

$$R = \frac{(C_o - C_e)}{C_o} \times 100 \quad (3)$$

where  $q_e$  is the amount of metal ions (mg g<sup>-1</sup>) adsorbed at the surface of samples,  $R$  (%) represents the percentage of ions removal,  $W$  is the weight (g) of sorbent used,  $V$  is the volume (L) of cobalt ion solution and  $C_o$ ,  $C_t$  and  $C_e$  are the concentrations (mg L<sup>-1</sup>) of cobalt solutions at the initial time, different time intervals, and at equilibrium, respectively.

For kinetic studies, a series of experiments were performed by altering the contact time from 1 to 240 min using 400 mg L<sup>-1</sup> of cobalt solution. The effect of adsorbent quantity on adsorption capacity was studied by changing the adsorbent dose from 20 to 1,000 mg at an initial concentration of adsorbate,  $C_o = 400$  ppm, and contact time 3 h at 25°C. For thermal analysis, experiments were carried out at a temperature ranging from 10 to 60°C. The effect of pH on adsorption capacity was examined by changing the pH of the cobalt ion solution from 2–13 at an initial concentration of adsorbate,  $C_o = 400$  ppm, contact time 3 h, and temperature 25°C.

### 2.6. Interference of foreign ions on adsorption capacity

To study the effect of foreign ions, 0.020 g of prepared sample was put in 40 mL of the solution containing 20 mL of cobalt ions solution (400 mg L<sup>-1</sup>) and 20 mL of each foreign ions solution (400 mg L<sup>-1</sup>) from KCl, CaCl<sub>2</sub>, FeCl<sub>3</sub>, ZnCl<sub>2</sub>, CuOOCCH<sub>3</sub>, and NiSO<sub>4</sub>. The sample solutions were stirred for an hour and filtered to remove the solid particles. To know the amount of adsorbed quantity on nanocomposites, UV absorbance (at 510 nm) of the filtrate was measured and the amount of adsorbed Co<sup>2+</sup> ions was calculated by using Eq. (2) [12,26].

### 2.7. Regeneration and recycling

This subsequent part of the study is concerned with the evaluation of the reusability and recycling of the synthesized materials several times. Briefly, 0.08 g of each type of the nanocomposite films was dipped in 20 mL of metal ions solution (400 ppm) and stirred for 2 h. After the time interval, the stirred solution was filtered, and the amount of metal ions adsorbed on the surface of samples was measured by the spectroscopic method at 510 nm. The adsorbents obtained on filter paper were washed with distilled water 3–4 times and dried in an oven at 50°C. The concentration of Co(II) ions desorbed by deionized water was measured by taking the UV absorbance of rinsed water (having desorbed Co(II) ions) at 510 nm. The next adsorption/desorption processes were proceeded by repeating a similar procedure until the color of the metal persists.

### 3. Results and discussions

#### 3.1. Characterization techniques

Fig. 1a represents the FTIR spectra of Algi, Algi+Chito, Cs90, Cc90, and CD90 samples. The prepared materials revealed a broadband that appeared at  $3,000\text{--}2,850\text{ cm}^{-1}$ , assigned to the C–H stretching vibration of  $-\text{CH}_3$  groups. The bands that appeared at  $1,031\text{--}1,010\text{ cm}^{-1}$  are produced by the C–O stretching vibrations of carbohydrate rings present in all materials. The broadband that appeared at  $3,484\text{--}3,010\text{ cm}^{-1}$  is assigned to stretching vibrations of H-bonded OH groups [27]. It is important to mention here that these bands (of OH groups) are not as intense in nanocomposites as in the starting materials suggesting the interaction between nanofillers and matrix molecules. The COOH groups of MWCNTs undergo electrostatic interactions and H-bonding between COOH, OH, and  $\text{NH}_2$  groups of Algi+Chito matrix molecules. Along with the possible interactions between two COOH groups of MWCNTs, the intensity of the OH group is reduced. The FTIR spectra of nanocomposites revealed intensive bands in the range of  $1,565\text{--}1,550\text{ cm}^{-1}$  assigned to the bending vibrations of N–H bonds (typical of amide groups). The presence of MWCNTs in nanocomposite films is confirmed by the C=C stretching frequencies of the graphene sheet that appeared at  $1,642\text{--}1,641\text{ cm}^{-1}$ . The effect of surfactants in dispersion and composite formation is not appreciably different than the non-surfactant medium.

Morphological features of adsorbents are studied by XRD analysis and shown in Fig. 1b. The experimental data suggested that the synthesized nanocomposites showed no prominent peak of an index except small XRD patterns

appeared which is an indication of amorphous structure. The slight diffraction pattern obtained in XRD spectra is attributed to crystallites that developed in amorphous nanocomposite networks by proper arrangement in polymeric chains. The inter-ionic interactions among nanofiller-matrix, nanofiller-nanofiller, and matrix-matrix molecules arranged the polymeric chains into a pattern and crystallites may develop. These crystallites diffracted the X-rays at  $2\theta = 35.6^\circ$ ,  $58.7^\circ$ ,  $62.7^\circ$  in Cs90,  $2\theta = 24^\circ$  in Cc90 and  $2\theta = 35^\circ$ ,  $42^\circ$  and  $55^\circ$  in CD90. The XRD results led us to conclude that on incorporating COOH-MWCNTs in the Algi+Chito matrix, an amorphous structure having some degree of arrayed polymeric chains is formulated.

TGA and DSC techniques are applied to determine the thermal behavior of prepared materials and results are given in Fig. 1c and d. The deflection in mass at  $20^\circ\text{C}\text{--}112.2^\circ\text{C}$  appeared on TGA curves, accompanied by an endothermic peak on DSC curves at  $56.99^\circ\text{C}$  correspond to the evaporation of entrapped water from the samples. This endothermic evaporation corresponds to a 10% loss in the mass of samples. The second step of thermal decomposition appeared at  $112.2^\circ\text{C}\text{--}153.7^\circ\text{C}$  is assigned to exothermic reaction (exothermic peak appeared at  $104.16^\circ\text{C}$ ) related to the removal of bonded water (3.64%). A subsequent fast and greater mass loss (55.22%) is observed at  $154^\circ\text{C}\text{--}403.4^\circ\text{C}$  and corresponds to the depolymerization, breakage of glycosidic, polyelectrolytic, and inter-ionic electrostatic linkages present between alginate-chitosan and COOH-MWCNTs. The process of deacetylation and deamination in chitosan polymer is also reported at this temperature [28]. Above  $400^\circ\text{C}$ , highly exothermic degradation reaction occurred at  $403^\circ\text{C}\text{--}501^\circ\text{C}$  and it is interpreted as caused by the mass

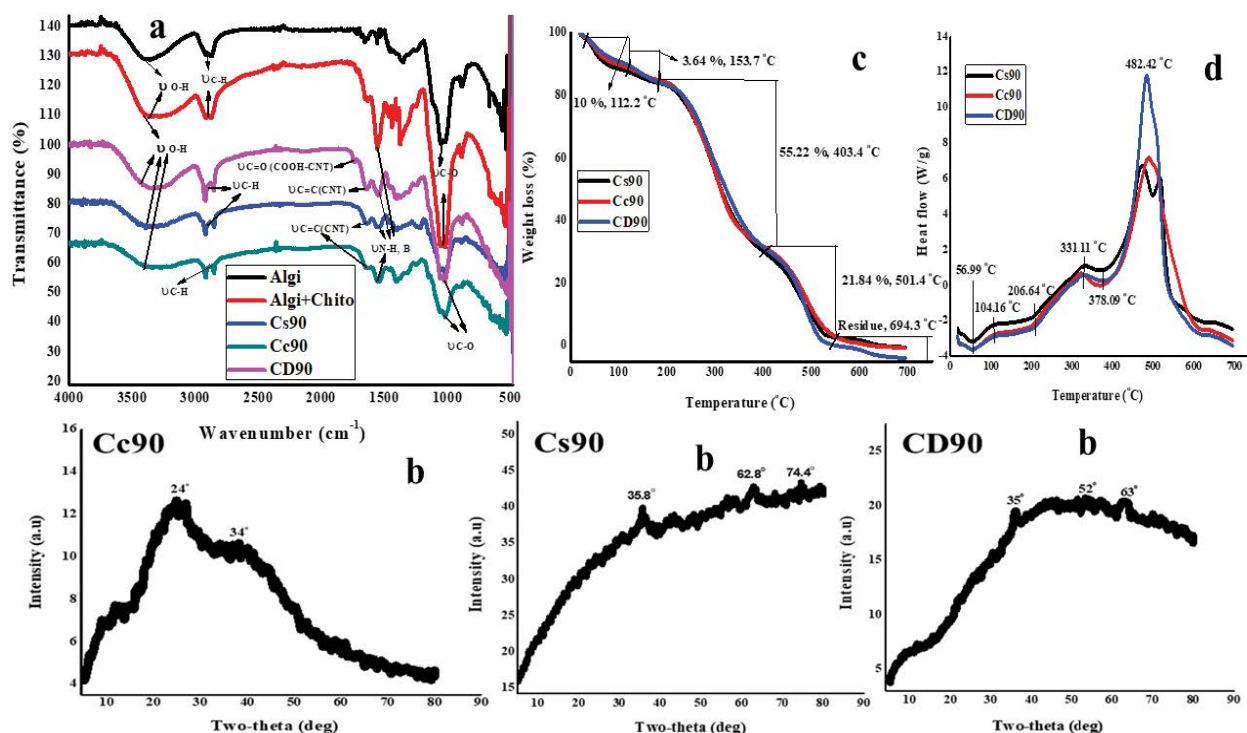


Fig. 1. (a) FTIR spectra of nanocomposites, (b) XRD spectra of nanocomposites, (c) TGA, and (d) DSC graphs of nanocomposites.

deflection of mannuronic acid, guluronic acid and gluconic acid of alginate-chitosan blend leads to the formation of acetic acid, formic acid, and butyric acid along with series of fatty acid [29]. This loss in mass contributes 21.84% in total deflection, the elimination of COOH groups in COOH-MWCNTs also occurs at this temperature [30]. It has been observed that in this exothermic degradation reaction, the DSC peak of CD90 released greater heat (heat flow 12 W/g) than surfactant-containing sorbents, Cs90, Cc90 (heat flow 6.5 W/g range). It is probably due to the greater rate of formation of small fatty acids during thermal degradation in CD90 sorbent than in Cs90 and Cc90 sorbents. At about 694.3°C complete (100%) thermal degradation occurred in nanocomposites. The comparison of synthesized nanocomposites with a reported alginate-chitosan blend showed that the alginate-chitosan matrix remained stable only at 300°C [30]. While the synthesized nanomaterials showed stability up to 694.3°C, suggesting the intermolecular interactions between nanofillers and Algi+Chito blend.

The surface area analysis of prepared samples was carried out by the BET technique. According to the obtained results, the nanocomposites showed BET area  $8.054 \pm 0.703 \text{ m}^2 \text{ g}^{-1}$ ,  $8.076 \pm 0.780 \text{ m}^2 \text{ g}^{-1}$ ,  $7.998 \pm 0.709 \text{ m}^2 \text{ g}^{-1}$  for Cs90, Cc90, and CD90 films with pore volume  $0.024 \pm 0.015 \text{ cm}^3 \text{ g}^{-1}$ ,  $0.032 \pm 0.014 \text{ cm}^3 \text{ g}^{-1}$ ,  $0.032 \pm 0.012 \text{ cm}^3 \text{ g}^{-1}$ , respectively. The involvement of nanofillers in composite formation leads to an increased specific surface area compared to Algi with BET area  $0.668 \pm 0.294 \text{ m}^2 \text{ g}^{-1}$ , pore volume  $0.005 \pm 0.000 \text{ cm}^3 \text{ g}^{-1}$ , and Algi+Chito having BET area  $3.165 \pm 0.497 \text{ m}^2 \text{ g}^{-1}$ , pore volume  $0.011 \pm 0.004 \text{ cm}^3 \text{ g}^{-1}$ . The pore diameter of nanocomposites is also larger

( $3.142 \pm 0.281 \text{ nm}$ ,  $3.253 \pm 0.283 \text{ nm}$ ,  $3.480 \pm 0.283 \text{ nm}$ ) than the starting materials ( $1.219 \pm 0.128 \text{ nm}$ ,  $2.060 \pm 0.140 \text{ nm}$ ). The incorporation of COOH-MWCNTs produced numerous cavities with large specific surface area and pore width, hence resulting in the formation of stable, interconnected, and porous nanocomposites. The role of nanoparticles in increasing the specific surface area of nanocomposites is according to the previously reported data [31]. The larger cavities and surface area provided advantageous conditions to adsorb the target substances and increased the adsorption rate.

The surface morphology of nanocomposites and starting materials was studied by SEM images (Fig. 2a–e) and TEM images (Fig. 2f and g). Both these images indicated the dispersed and even distribution of nanofillers in the alginate-chitosan matrix. TEM image revealed the scattered and un-agglomerated nature of COOH-MWCNTs in the Algi+Chito matrix, indicating the usefulness of sonic waves for the complete dispersion of nanofillers in the polymeric matrix. The large particles in the TEM image were un-dissolved matrix molecules that agglomerated and appeared. The SEM analysis revealed that the surface of Algi and Algi+Chito is smooth while the surfaces of nanocomposites are grooved and uneven indicating the dispersion of nanofillers in polymeric chains. Results showed that the SEM images of sorbents having surfactants are not different from the non-surfactants containing sorbent (CD90) exhibiting the little effect of solving media on dispersion where the two-dispersing media are surfactants and non-surfactants. They showed almost similar behavior in dispersion. The similar nature of dispersion in both types of sorbents was also confirmed by BET area and porosity, as nanocomposites

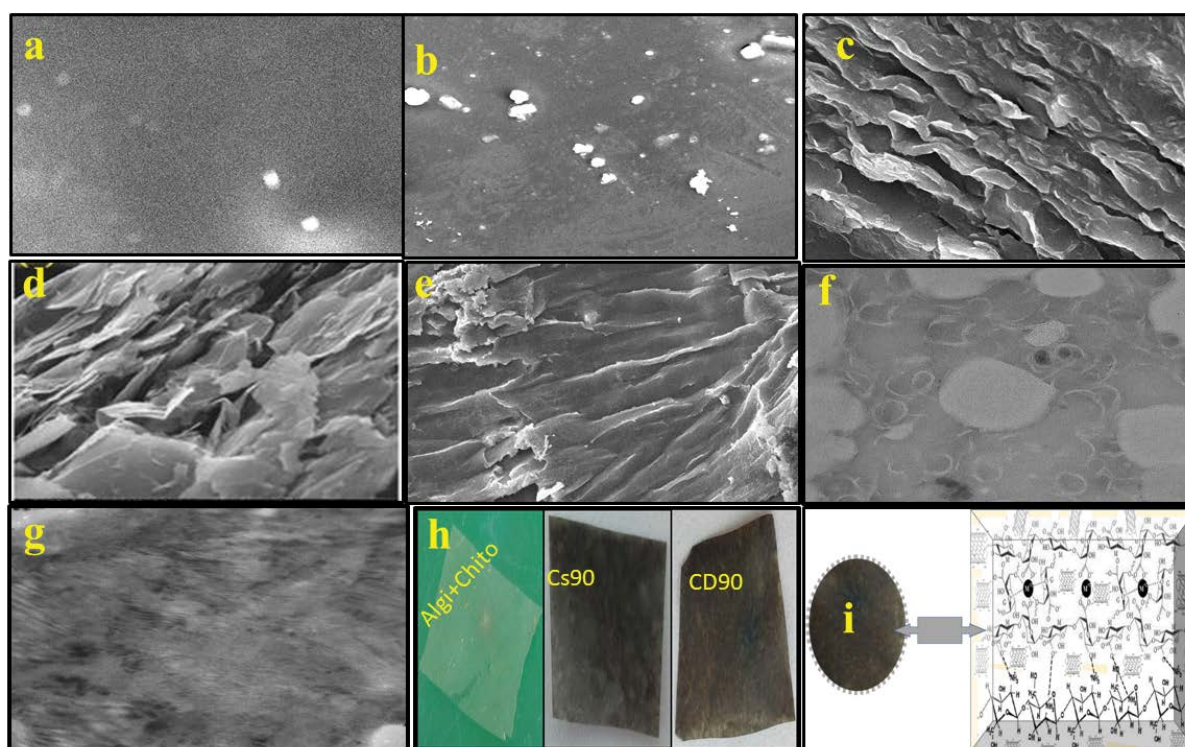


Fig. 2. SEM images of (a) Algi, (b) Algi+Chito, (c) Cc90, (d) Cs90, (e) CD90 films, (f and g) TEM images of nanocomposites, (h) photographic images of synthesized samples, and (i) proposed interaction pattern in the nanocomposite.

having BET area ( $7.998 \pm 0.709$ ,  $8.054 \pm 0.703$ ,  $8.076 \pm 0.780$ ) of CD90, Cs90, Cc90, respectively. The porosity of CD90 is 0.778 (calculated by volume fractions) in comparison with Cs90 (0.748) and Cc90 (0.664), respectively while the porosity of Algi and Algi+Chito was observed to lie within the range of 0.427 and 0.577, respectively.

### 3.2. Swelling measurements

Prepared nanocomposites (Cs90, Cc90, CD90) were evaluated by swelling capacity and compared with starting materials; Algi, Algi+Chito in various dispersing media [24]. Due to the presence of electrostatic interactions (H-bonding between COOH-MWCNTs and COOH, OH, and  $\text{NH}_3$  groups of Algi+Chito), the nanocomposites showed lower values of swelling compared to pristine Algi and Algi+Chito. Moreover, these interactions are also responsible to give a more stable nature to nanocomposites, while starting materials disintegrated after a specific period. The obtained results are in accordance with the previously reported data [15].

### 3.3. Adsorption of metal ions

Synthesized materials were checked for adsorption ability with cobalt metal ions. The adsorption capacity of films was evaluated by changing the parameters like

contact time, pH, temperature, and dosage of the adsorbate. The effects of these factors are illustrated here.

#### 3.3.1. Effect of contact time

The amount of  $\text{Co}^{2+}$  metal ions adsorbed on the prepared materials was measured against the time of contact between adsorbate and adsorbent to reach the time of equilibrium. Fig. 3a indicates rapid adsorption in the first 20 min, which leads to 35%–40% of metal ion removal. The remaining 60% uptake of ions required 218 min to reach the equilibrium. The Algi and Algi+Chito adsorbed only 33.3% and 50% metal ions, respectively in about an hour and then disintegrated. The increased rate of adsorption in nanocomposite films is attributed to the greater specific surface area, stability, and presence of reactive centers on nanofillers. Awual et al. studied a broad range of pollutants and found that the reactive centers/open functionality of reinforcing materials increased the adsorption capacity of sorbents at optimum conditions [9,10,26]. The fast up-taking of adsorbate during the initial time of contact is interpreted as in the beginning due to the porous nature of nanocomposites, a great number of vacant sites for physical as well as chemical adsorption. As time proceeded, the available vacant sites showed the tendency to diminish, and the adsorption process slowed down. Thus, on reaching the equilibrium, there was no vacant site on the surface of nanocomposite

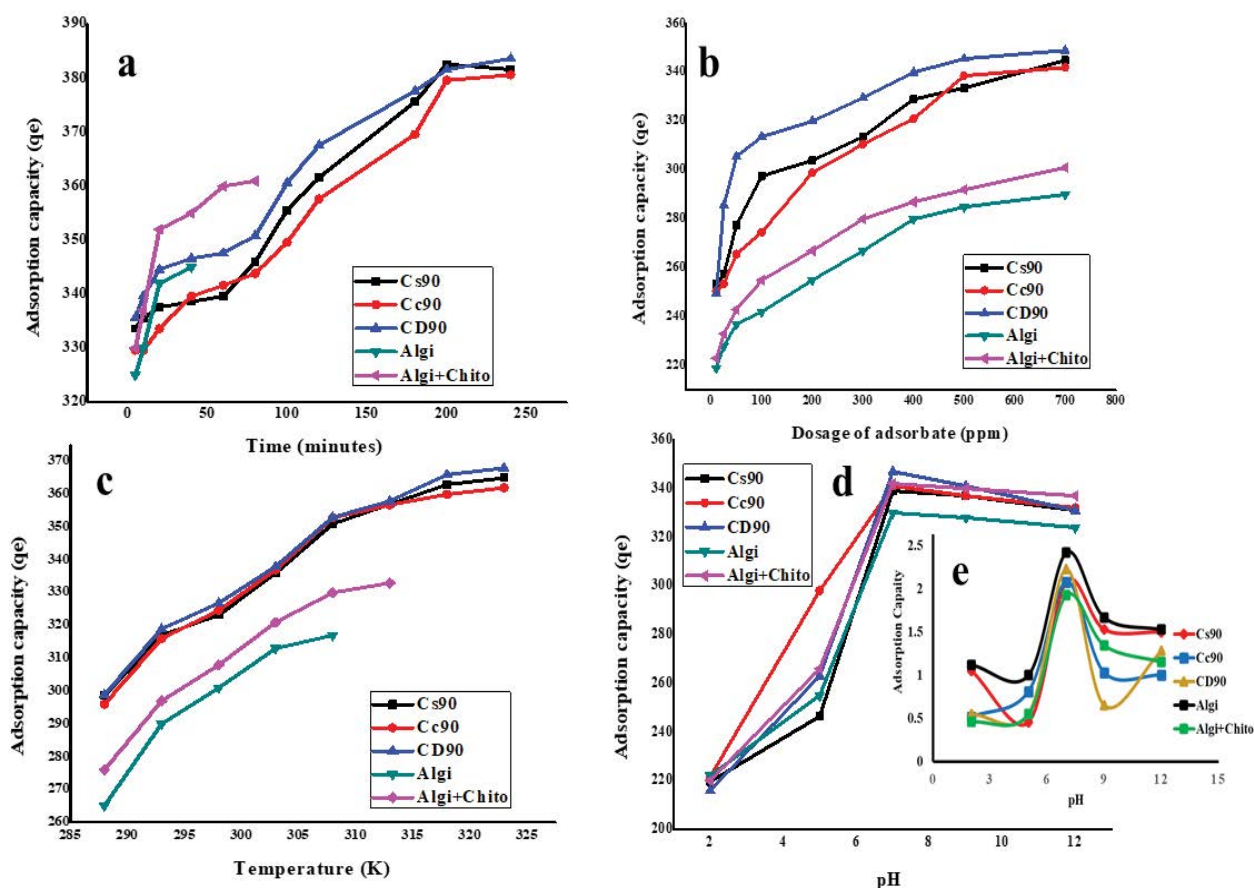


Fig. 3. Effect of (a) contact time, (b) concentration of adsorbate, (c) temperature, and (d and e) pH on adsorption capacity of samples.

for intermolecular diffusion of metal ions (unchanged in  $q_e$  values) [2]. In the presence of surfactants, no prominent difference in  $q_e$  values was obtained. Only a slight difference (decreasing trend) in adsorption capacity of films (Cs90, Cc90) was obtained which may be due to the decrease in porosity than non-surfactant-containing film (CD90).

3.3.1.1. Adsorption kinetics

To know the rate of adsorption, amount of adsorbate uptake, and time for maximum adsorption, three kinetic models namely pseudo-first-order, pseudo-second-order, and intraparticle diffusion model were applied on sorption data.

The basic assumption of pseudo-first-order is that the adsorption of adsorbate on the surface of the adsorbent is proportional to the number of available vacant sites. While pseudo-second-order assumes that the amount of cobalt ions adsorbed on the surface of prepared films is proportional to the square of vacant sites [18]. Weber and Morris assume in intraparticle diffusion that this type of diffusion is a rate-determining step of the adsorption process. The linear forms of pseudo-first-order, pseudo-second-order, and rate-determining step are represented by Eqs. (4)–(6) [32].

$$\ln(q_e - q_t) = \ln q_e - k_1 t \tag{4}$$

$$\frac{t}{q_t} = \frac{1}{k_2 q_e^2} + \frac{t}{q_e} \tag{5}$$

$$q_t = k_i t^{0.5} + C \tag{6}$$

where  $q_e$  and  $q_t$  ( $\text{mg g}^{-1}$ ) are the amount of  $\text{Co}^{2+}$  metal ions on the surface of samples at equilibrium and at time  $t$ , respectively.  $k_1$  is the Lagergren rate constant ( $\text{min}^{-1}$ ),  $k_2$  ( $\text{g mg}^{-1} \text{min}^{-1}$ ) is the rate constant for second-order,  $k_i$  ( $\text{mg g}^{-1} \text{min}^{-0.5}$ ) is an intraparticle diffusion rate constant and  $C$  is the effect of boundary layer thickness.

The statistical criteria used to determine the best fitting of kinetic models on the experimental sorption data depends upon the difference between experimental and calculated adsorption capacities ( $q_e$ ) and the value of squared multiple regression coefficients ( $R^2$ ). The plots of  $\ln(q_e - q_t)$  vs.  $t$  and  $t/q_t$  vs.  $t$  (shown in Fig. 4a and b) are used to calculate the constants of pseudo-first-order and pseudo-second-order kinetic models and are summarized in Table 1. The values of the regression coefficient ( $R^2 = 0.999$ ) obtained by applying the pseudo-second-order kinetic model indicate the best fitting of this model on the study of adsorption of  $\text{Co}^{2+}$  metal ions compared to the pseudo-first-order model. Moreover, the values of adsorption capacities ( $q_e$  experimental) are closer to the ( $q_e$  calculated) in pseudo-second-order than the first-order. As the nanocomposites (Cs90, Cc90, CD90) have 381, 380, and 383  $\text{mg g}^{-1}$  the values of experimental adsorption capacities (Fig. 3a). Alginate-based materials are also reported to adsorb various adsorbates preferably by following pseudo-second-order kinetics [33].

At the subsequent stage of the study, the mechanism involved in the intraparticle diffusion process was determined by plotting the graph of  $q_t$  vs.  $t^{0.5}$ . If the obtained

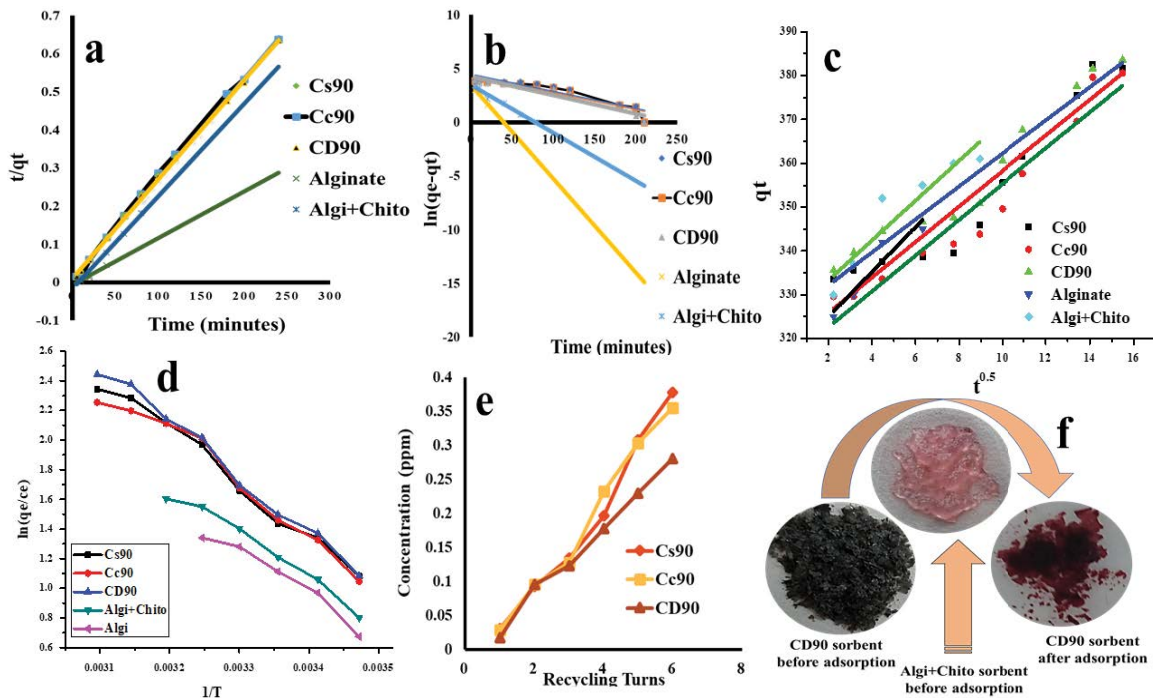


Fig. 4. (a) Linear curve fitting of pseudo-first-order, (b) pseudo-second-order and (c) intraparticle diffusion kinetic models on adsorption of  $\text{Co}^{2+}$  ions on the synthesized samples, (d) plot of thermodynamics used to determine the entropy and enthalpy of samples, (e) concentration of  $\text{Co(II)}$  ion obtained after each recycling turn in rinsed water, (f) shapes of films before and after adsorption of  $\text{Co(II)}$  ions.

Table 1  
Kinetics model parameters for Co(II) ions adsorption on prepared samples

Samples	Cs90	Cc90	CD90	Algi	Algi+Chito
<b>Pseudo-first-order</b>					
$q_{e(\text{calc})}$ mg g <sup>-1</sup>	81.17	75	68.5	32.07	32.82
$k_1 \times 10^{-2}$ (min <sup>-1</sup> )	1.58	1.59	1.7	8.75	4.49
$R^2$	0.8521	0.8971	0.895	0.895	0.944
<b>Pseudo-second-order</b>					
$q_{e(\text{calc})}$ mg g <sup>-1</sup>	384.7	370.3	384.6	212.9	327.6.6
$k_2 \times 10^{-4}$ (g mg <sup>-1</sup> min <sup>-1</sup> )	5.6	9.1	7.1	2.0	3.3
$R^2$	0.998	0.997	0.999	0.987	0.988
<b>Intraparticle diffusion</b>					
$k_i$ (mg g <sup>-1</sup> min <sup>0.5</sup> )	4.04	4.08	3.76	5.11	4.45
$C$ (mg g <sup>-1</sup> )	317.7	314.4	324.6	314.7	324.2
$R^2$	0.90	0.94	0.95	0.90	0.881

plot has crossed form and passes through the origin, then the intraparticle diffusion is the sole rate-limiting step. However, if this plot has passed through the origin and having some values of intercept ( $C$ ), it indicates the thickness of the boundary layer (Table 1). In the current study, the values of  $k_i$  and  $C$  were obtained by the slope and intercept of the plot  $q_t$  vs.  $t^{0.5}$  respectively. The results showed that linear plots have not crossed origin (Fig. 4c) and the mechanism involved is not sole limiting. Rather, some other mechanism may play an important role. Most probably, the surface adsorption (pseudo-second-order) and intraparticle diffusion take place simultaneously.

### 3.3.2. Effect of adsorbate dose

The effect of the initial concentration of Co(II) ions on the  $q_e$  (mg g<sup>-1</sup>) values of samples were investigated by using a fixed amount of adsorbents (0.02 g) at 25°C. Fig. 3b indicates that initially, the rate of adsorption capacity (mg g<sup>-1</sup>) increased with increasing concentration. By increasing the concentration of Co(II) ions from 10 ppm to 700 ppm, the maximum  $q_e$  values were obtained at about 500 ppm, and later these values remained almost constant. This was likely due to the presence of many active centers and voids at the beginning of the adsorption process which became saturated at an equilibrium point [33]. When the concentration of adsorbate was further increased (from 500 to 700 ppm) the saturated centers were unable to further uptake adsorbate and thus  $q_e$  values remained constant. The obtained results confirm the literature data [18]. Nanocomposites (Cs90, Cc90, CD90) showed the highest  $q_e$  values (348, 345, and 350 mg g<sup>-1</sup>) due to stable and more reactive nature compared to Algi (290 mg g<sup>-1</sup>) and Algi+Chito (301 mg g<sup>-1</sup>) films. The involvement of surfactants did not significantly affect adsorption capacities values. Only a slight difference was observed.

#### 3.3.2.1. Adsorption isotherms

To study the amount of Co<sup>2+</sup> ions adsorbed at the surface of samples and concentration of adsorbate deposited

at equilibrium, two equilibrium isotherms, called Langmuir and Freundlich isotherms were applied.

The Langmuir model is based on assumption that the adsorption process takes place on the energetically uniform active surface and adsorbate forms a saturated monolayer with the thickness of a molecule. The linear and nonlinear forms of the Langmuir model are shown in Fig. 5a and b, respectively [18].

Linear expression:

$$\frac{C_e}{q_e} = \frac{1}{k_L q_m} + \frac{C_e}{q_m} \quad (7)$$

Nonlinear expression:

$$q_e = \frac{k_L \times q_m \times C_e}{1 + k_L \times C_e} \quad (8)$$

where  $k_L$  is a constant called Langmuir constant,  $C_e$  (mg L<sup>-1</sup>) is the concentration of adsorbate at equilibrium,  $q_e$  and  $q_m$  are the adsorption capacities (mg g<sup>-1</sup>) at equilibrium and maximum, respectively.

Freundlich model theoretically assumes the multilayer adsorption of adsorbate on the heterogeneous surface having different energy of adsorption. The empirical linear and nonlinear equations of the Freundlich isotherm model are shown in the following equations [18].

Linear expression:

$$\ln q_e = \ln k_F + \frac{1}{n} \ln C_e \quad (9)$$

Nonlinear expression:

$$q_e = k_F C_e^{1/n} \quad (10)$$

where  $k_F$  and  $n$  are adsorption equilibrium constants for Freundlich isotherm, indicate the adsorption intensity and

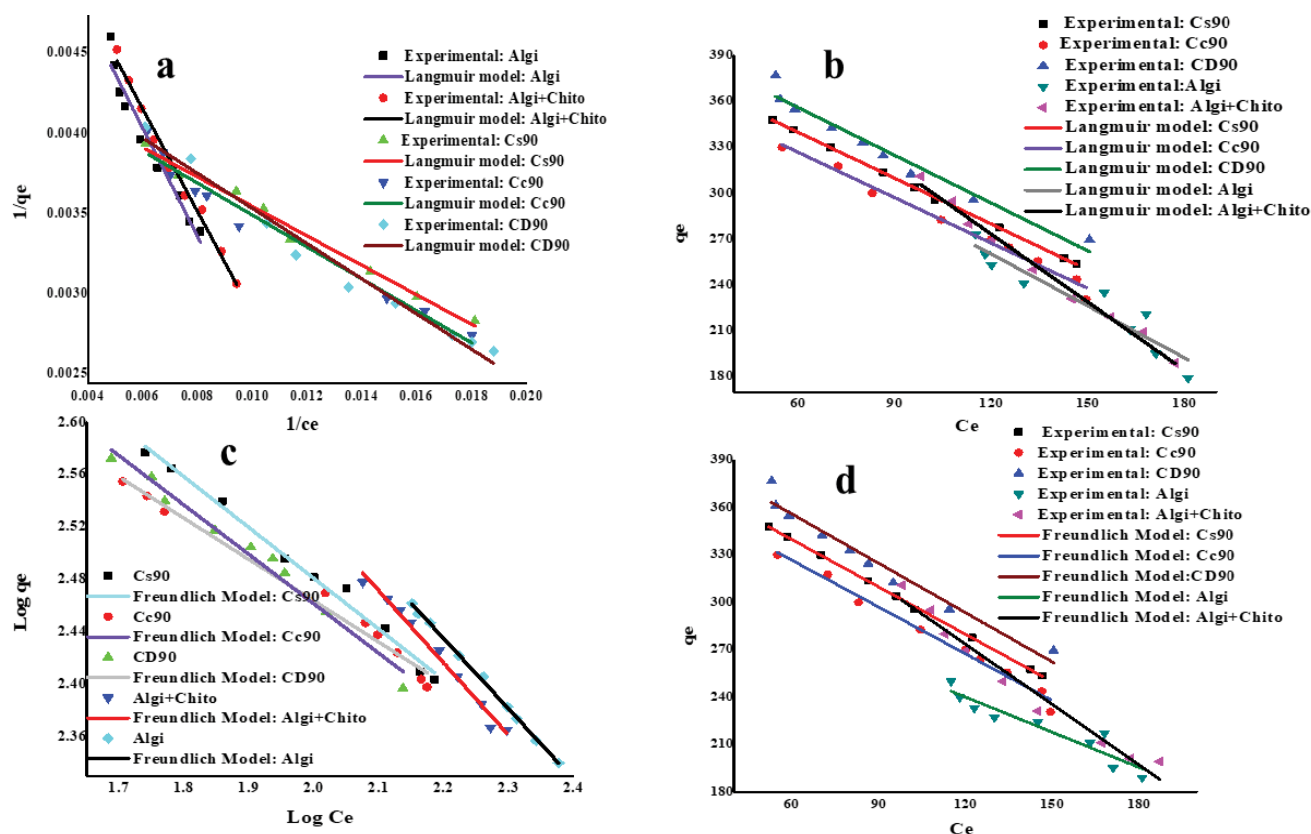


Fig. 5. Linear and nonlinear curves fitting on (a and b) Langmuir model; (c and d) Freundlich model, respectively.

heterogeneous factor. Lesser is the value of  $n$ , the greater will be the interaction between adsorbate and adsorbent.

The choice of a model to explain the equilibrium adsorption on the surface of nanocomposites depends upon the quality of fitting to experimental data, and by the value of  $R^2$  (regression coefficient). To determine the values of  $k_L$  and  $q_m$  in the Langmuir model and  $k_f$  and  $n$  in the Freundlich model, plots of  $C_e/q_e$  vs.  $C_e$  and  $\ln q_e$  vs.  $\ln C_e$  are taken, respectively. The slopes and intercept values of drawn plots give the values of constants. It was evident from the values of the correlation coefficient and the sum of squared error (SSE) statistical analysis (Table 2) that the Langmuir linear is the best isotherm model to explain the equilibrium adsorption process than the Freundlich model.

According to the data presented in Table 2, it is concluded that the adsorption of cobalt metal ions on the surface of prepared samples is of the Langmuir type. The value of the correlation coefficient obtained by linear fitting on the Langmuir model was 0.995, 0.994, 0.998 for Cs90, Cc90, and CD90 nanocomposites while these values were 0.994 for Algi and Algi+Chito films. In a comparison of linear fit with the Freundlich model, the  $R^2$  value was poorer, and it varied from 0.92 to 0.98. Moreover, the maximum monolayer adsorption capacities ( $q_m$ ) obtained in the Langmuir model were 350–356  $\text{mg g}^{-1}$  for nanocomposites, which were closer to the experimental values ( $q_e$ ) 345–349  $\text{mg g}^{-1}$ . These results proved the homogeneous adsorption of cobalt metal ions on the active surfaces of synthesized nanocomposites.

A dimensionless factor called the separation factor ( $R_L$ ) is used to determine the suitability of the Langmuir model than the Freundlich model. The mathematical expression of this factor is represented in Eq. (11) [33].

$$R_L = \frac{1}{1 + K_L C_o} \quad (11)$$

The factor  $R_L$  is called the separation factor,  $K_L$  is the Langmuir constant related to the heat of adsorption and  $C_o$  is the initial concentration ( $\text{mg L}^{-1}$ ) of cobalt metal ions.

The values of  $R_L$  indicate that the nature of adsorption is either unfavorable ( $R_L > 1$ ), linear ( $R_L = 1$ ) or irreversible ( $R_L = 0$ ). In the current study, the values of  $R_L$  in the Langmuir model lied in the range of 0.06, 0.07, 0.05, 0.11, 0.10 for Cs90, Cc90, CD90, Algi, and Algi+Chito samples, respectively, that ranged between 0 and 1, while in Freundlich 'n' values were greater than 1 indicating unfavorable adsorption.

The nonlinear approach was also used to know about the maximum adsorption of cobalt(II) ions on the synthesized sorbents in which both Langmuir and Freundlich models were interestingly studied in a nonlinear way [34]. The corresponding isotherm parameters, like regression coefficients and isotherm constants, have been shown in Fig. 5 and calculated values have been summarized in Table 2.  $R^2$  values indicated that both nonlinear Freundlich and Langmuir models were less fitted than the linear

Table 2  
Equilibrium isotherm (linear and nonlinear) constants and values of  $\chi^2$  for Co(II) ions adsorption on prepared samples

Samples	Cs90	Cc90	CD90	Algi	Algi+Chito
<b>Freundlich (linear)</b>					
$k_f$	272	284	288	198	222
$n$	1.47	1.44	1.40	2.34	1.72
$R^2$	0.973	0.981	0.922	0.971	0.960
$\chi^2$	19.59	11.84	12.92	42.74	28.11
<b>Langmuir (linear)</b>					
$q_m$	350.8	352.0	356.2	287.29	299.49
$K_L \times 10^{-2}$	3.8	3.2	4.4	1.9	2.1
$R^2$	0.995	0.994	0.998	0.994	0.994
$\chi^2$	0.095	0.284	0.145	0.025	0.007
<b>Freundlich (nonlinear)</b>					
$k_f$	292	286	298	204	243
$n$	1.1	1.0	1.1	1.3	1.4
$R^2$	0.965	0.976	0.968	0.985	0.980
$\chi^2$	9.61	10.96	8.72	36.25	13.84
<b>Langmuir (nonlinear)</b>					
$q_m$	298.2	299.7	312.9	191.20	209.43
$K_L \times 10^{-3}$	2.5	2.4	2.4	2.1	3.2
$R^2$	0.975	0.984	0.968	0.974	0.976
$\chi^2$	7.344	5.971	4.164	51.050	40.030

isotherms. However, the adsorption capacity value calculated by the nonlinear Freundlich model was close to experimental values than the linear – Freundlich model. Thus, it can be concluded from the results that the adsorption of cobalt metal ions was a monolayer and of homogeneous type.

### 3.3.2.2. Error analysis

The fitness of the isotherm model in depicting the adsorption of cobalt metal ions on nanocomposites was further confirmed by the sum of squared error (SSE) statistical analysis. The standard expression of this analysis is represented in Eq. (12) [32].

$$SSE(\chi^2) = \sum_{i=1}^n \frac{(q_{e(\text{calc})} - q_{e(\text{Exp})})^2}{q_{e(\text{calc})}} \quad (12)$$

where  $q_{e(\text{calc})}$  is the calculated and  $q_{e(\text{Exp})}$  is the experimental values of adsorption capacities ( $\text{mg g}^{-1}$ ). The values of  $\chi^2$  provide an insight into the fitness of any model, the smaller the values of  $\chi^2$ , the greater will be convergence to experimental data, and the greater the model favorable. By

applying the SSE expression, the obtained results for linear as well as nonlinear isotherms have been summarized in Table 2. Results indicate that chi-square ( $\chi^2$ ) values are lower in Langmuir linear model with greater  $R^2$  which can generate a satisfactory fit to the experimental data compared to the Freundlich model. The saturation amounts in the Freundlich model obtained using nonlinear regression are also to some extent lower compared to the linear Freundlich model. This indicates the suitability of the nonlinear Freundlich model to explain the equilibrium data.

### 3.3.3. Effect of temperature

The varying effect of temperature on adsorption of cobalt metal ions on the active surface of materials was studied at constant adsorbate concentration ( $400 \text{ mg L}^{-1}$ ), adsorbent amount ( $0.02 \text{ g}$ ), and neutral pH. Results obtained by this analysis (Fig. 3c) indicated the increase in  $q_e$  values by increasing temperature, suggesting that the adsorption of cobalt ions is an endothermic process. Experimental data showed that by increasing the temperature from 288 to 323 K, values of  $q_e$  increased from 298 to  $365 \text{ mg g}^{-1}$ ,  $362 \text{ mg g}^{-1}$ ,  $368 \text{ mg g}^{-1}$ ,  $317 \text{ mg g}^{-1}$ , and  $333 \text{ mg g}^{-1}$  for Cs90, Cc90, CD90, Algi, and Algi+Chito, respectively. Greater values of adsorption capacities at higher temperatures are attributed to the high mobility of adsorbate ions due to declined solution viscosity and greater swelling in films with more segmental motion. At lower temperatures, all the metal ions may not have the ability to penetrate and interact with adsorbent molecules depending on the energy of interaction between them. On an increase in temperature, the activation energy of a sufficient number of cobalt ions increased and interacted with the active surface of adsorbents, lead to increased adsorption capacity. Films of nanocomposites (Cs90, Cc90, CD90) remained stable at high temperature and gave maximum values ( $365$ ,  $362$ , and  $368 \text{ mg g}^{-1}$ ) of adsorption capacities in comparison with Algi and Algi+Chito ( $317$  and  $333 \text{ mg g}^{-1}$ ) which disintegrated at  $\sim 308$  and  $313 \text{ K}$ . The films having surfactants did not behave differently than the films with no surfactant at various temperatures, indicating a little effect of surfactants on the adsorption process.

### 3.3.3.1. Thermodynamic studies

Thermodynamic parameters are very important to determine the inherent changes in the adsorption process at various temperature ranges. Gibbs free energy ( $\Delta G^\circ$ ), entropy ( $\Delta S^\circ$ ), and enthalpy ( $\Delta H^\circ$ ) (thermodynamic parameters) are determined by the following expressions [32].

$$k_c = \frac{q_e}{C_e} \quad (13)$$

$$\Delta G^\circ = -RT \ln K_c \quad (14)$$

$$\ln K_c = \frac{\Delta S^\circ}{R} - \frac{\Delta H^\circ}{RT} \quad (15)$$

Table 3  
Thermodynamic parameters for Co(II) ions adsorption using the prepared samples

Types of samples	Thermodynamic parameters		
	$-\Delta G^\circ$ (kJ mol <sup>-1</sup> )	$\Delta H^\circ$ (kJ mol <sup>-1</sup> )	$\Delta S^\circ$ (kJ mol <sup>-1</sup> )
Cs90	515.927	3,531	13.35
Cc90	511.15	3,363	12.78
CD90	530.10	3,726	14.04
Algi	357.01	2,926	10.83
Algi+Chito	413.73	2,939	11.06

$$\Delta G^\circ = -RT \ln K_c = -RT \frac{\Delta S^\circ}{R} - \frac{\Delta H^\circ}{RT} \quad (16)$$

where  $K_c$  is the distribution coefficient,  $R$  is a general gas constant (8.314 J K<sup>-1</sup> mol<sup>-1</sup>),  $T$  is the temperature (K).

The values of Gibbs free energy (kJ mol<sup>-1</sup>) are obtained by solving the equation '16' at 303.15 K, while the values of  $\Delta S^\circ$  and  $\Delta H^\circ$  are obtained from the intercept and slope of the plot between  $\ln q_e/C_e$  vs.  $1/T$  (Fig. 4d).

Table 3 illustrates the calculated values of thermodynamic parameters. Negative values of  $\Delta G^\circ$  indicated the feasibility and spontaneous nature of adsorption of cobalt metal ions on films. Nanocomposite sorbents (Cs90, Cc90, CD90) showed higher values (515.927, 511.15, and 530.10 kJ mol<sup>-1</sup>, respectively) of  $\Delta G^\circ$  than Algi (357.01 kJ mol<sup>-1</sup>) and Algi+Chito (413.73 kJ mol<sup>-1</sup>) films. The standard enthalpy of reaction adopted a positive value, which indicates that the adsorption of cobalt ions is an endothermic process. The endothermic nature of the adsorption process is confirmed by increasing the adsorption capacity with increased temperature, attributed to a higher degree of spontaneity at higher temperatures. Positive values of  $\Delta S^\circ$  (13.35, 12.78, 14.04, 10.83, and 11.06 kJ mol<sup>-1</sup>) suggest that the organization of the cobalt ions in the solid-solution interface becomes more random and is linked with the movement of water molecules adsorbed on the sorbents. Thus, the adsorption of cobalt ions increased the degree of disordering of water molecules at the solid-state/liquid interface and favors the adsorption of metal ions. Obtained results confirmed the previously conducted studies on the adsorption of other adsorbates on several adsorbents [18].

### 3.3.4. Effect of pH

Change in pH significantly affects the values of adsorption capacities due to the chemical speciation of the surface of the adsorbents. The behavior of all the synthesized materials (starting materials and nanocomposites) was the same, that is, lesser adsorption capacities in acidic and basic pH and greater in neutral pH (Fig. 3d). In a highly acidic medium (pH 2), all the synthesized films showed the least values of adsorption capacity (from 216 to 222 mg g<sup>-1</sup>). On changing the pH from acidic to neutral, the values of  $q_e$  increased and became maximum at 7 pH. In a basic medium (pH 10–13) again decline in  $q_e$  values was obtained, but

this decreasing trend in  $q_e$  values is not as prominent as obtained in an acidic medium. To obtain a significant difference in results, the standard deviation (s. d) was taken on the mean values of adsorption capacities at various pH (Fig. 3e). For the most effective sorbents, Cs90, Cc90, and CD90, the sorption capacity decreased from 339 mg g<sup>-1</sup> (s. d. 2.08) to 219 mg g<sup>-1</sup> (s. d. 1.05) by changing the pH from 7 to 2 and 339 mg g<sup>-1</sup> (s. d. 2.08) to 331 mg g<sup>-1</sup> (s. d. 1.4) by varying from 7 to 13. Starting films have a similar trend in sorption capacities but with little adsorbing abilities.

In an acidic medium, due to the protonation of free (the groups that are not involved in bonding between carbohydrates) COO<sup>-</sup> group of alginates and NH<sub>2</sub> group of chitosan, H-bonding and other electrostatic forces of attraction created in sorbents, which led to more convoluted structure with little pathways for diffusion. Moreover, in an acidic medium, electrostatic repulsion created between protonated groups of films and positively charged cobalt ions, an adsorbed layer of cobalt metal ions pushed away from the surface of nanocomposites and thus collectively decreased the sorption capacities. On shifting the pH from acidic to neutral, deprotonation of carboxylate groups and ammine groups followed by negative-negative repulsions caused the expansion in nanocomposite materials with greater access to intermolecular diffusion. While, in basic pH, again lower values in  $q_e$  were observed and are explained by the "charge screening effect" by metal ions of the basic medium. Sodium ions of NaOH (ions of basic medium) competed with Co<sup>2+</sup> ions (ions of adsorbate) to react with carboxylate groups of nanocomposites and entered pores. Consequently, a lesser quantity of Co<sup>2+</sup> ions was adsorbed on the surface of the synthesized sorbents.

### 3.4. Effect of foreign ions on adsorption capacity

Foreign ions affect and interfere with the sorption capacities of synthesized nanocomposites. To measure the effect of foreign ions, 20 mL of each of the metal salt solution (400 mg L<sup>-1</sup>) from K(I), Ca(II), Fe(III), Zn(II), Cu(II), and Ni(II) was investigated along with the Co(II) ions (400 mg L<sup>-1</sup>) and adsorption capacity was measured (Table 4) at 25°C and 7.0 pH. The experimental data showed that all the ions interfered with the adsorption process and competed with Co<sup>2+</sup> ions to adsorb on the surface of sorbents. This behavior is attributed to a cross-linking reaction between Na<sup>+</sup> ions of guluronic acid (G-block) and polyvalent ions, which lead to a characteristic egg-box structure [17]. In divalent ions, Ca<sup>2+</sup> showed the maximum capacity to absorb and reduced the  $q_e$  values of Co(II) ions from 345 to 147 mg g<sup>-1</sup> for CD90 sorbents. Similarly, in Cs90 and Cc90 sorbents,  $q_e$  values decreased from 340 and 342 mg g<sup>-1</sup> to 143 and 141 mg g<sup>-1</sup>, respectively. The highest ability of Ca<sup>2+</sup> ions to interact with COO<sup>-</sup> ions of alginate and displace the H<sup>+</sup> ions and Na<sup>+</sup> ions, attributed to low electropositivity and high reactivity of calcium ions than the other divalent ions. Trivalent and monovalent ions (Fe<sup>3+</sup> and K<sup>+</sup> ions) also have a considerable tendency to interact with reactive centers of alginate-chitosan/CNTs composites. Hence, the results suggested that the prepared sorbents are not specific for Co<sup>2+</sup> pollutants and can be used to remove various other ions from the wastewater. Our results for the interference of

foreign ions with Co(II) ions to compete with non-selective adsorption are also according to another study [2].

### 3.5. Regeneration and recycling

Regeneration or recycling is an important parameter that defines the demand for any new synthesis at the industrial level. The reusability of synthesized materials was practiced continuously by the adsorption/desorption process successfully six times. For each turn, 400 mg L<sup>-1</sup> of cobalt ion solution was used by using 0.08 g of the sorbent at 25°C. The sample was immersed in an adsorbate solution and stirred continuously to obtain the equilibrium adsorption. Then the samples were filtered and washed several times (3–4) with deionized water. The sorbents were dried in an oven (at 50°C) and used for the recycling process. The amount of Co<sup>2+</sup> ions adsorbed and desorbed (desorbed by deionized water) in each recycling turn is indicated by Table 4 and Fig. 4e. Results indicated that in the regeneration cycles from 1–6, the nature of adsorption capacity remained unaffected even after the six-run and lied in the range of 247–289 mg g<sup>-1</sup> for three types of sorbents. However, the pattern of adsorption was not regular and, in these cycles, no increasing or decreasing trend was observed. The greater adsorption values in repeated

cycles are due to greater reactive centers on the surface of nanocomposite films and greater inter-ionic and Van der Waal's attraction among Co<sup>2+</sup> ions. While the concentration of Co<sup>2+</sup> ions desorbed in each recycling turn was increased from cycle 1 to cycle 6. After reaching the 6th recycling time, nanocomposites sorbents became fully saturated and were unable to adsorb more metal ions. While the samples of starting materials, that is, Algi and Algi+Chito became flimsy in the first process of adsorption and were unable to be used again and again in the recycling process (Fig. 4f).

### 3.6. Comparison with other studies

The sorption capacity of synthesized sorbents is compared with the literature values of other alginate-based sorbents [2,35–40] and has been enlisted in Table 5. The proposed nanostructure of sorbents can be compared with other relevant studies. The greater adsorption capacity and subsequent regenerative cycles make the sorbents the most promising thing to be used in industries because of their being economical. Other alginate-based sorbents are also known to be used in heavy metals removal, but these showed lower adsorption capacity and had lesser turns of regenerative cycles. In the present study, sorbents showed higher values of adsorption capacity and were evaluated

Table 4  
Adsorption capacity of Co(II) ions in the presence of foreign ions and in recycling turns

S. No.	Types of films	Adsorption capacities ( $q_e$ ) in the presence of foreign ions					
		Cu <sup>2+</sup>	Ni <sup>2+</sup>	Zn <sup>2+</sup>	Ca <sup>2+</sup>	Fe <sup>3+</sup>	K <sup>+</sup>
1	Cs90	185	213	183	147	172	169
2	Cc90	181	199	177	143	169	167
3	CD90	189	207	179	141	170	170
S. No.	Types of films	Adsorption capacity for each recycling turn					
		First	Second	Third	Fourth	Fifth	Sixth
1	Cs90	273	221	239	283	247	278
2	Cc90	253	265	271	267	289	287
3	CD90	287	249	269	277	285	279

Table 5  
Comparison of  $q_{max}$  of alginate-based sorbents for heavy metal ions removal

Type of adsorbents	$q_{max}$ (mg g <sup>-1</sup> )	Metal ions	Recycling turns	References
Alginate/GO	56.49	Mn(II)	Seven	[35]
Alginate/GO aerogel	98.0	Cu(II)	One	[36]
Alginate/Hydroxyapatite CONH <sub>2</sub> -CNTs	347.8	Co(II)	One	[2]
Alginate/Nanographite	11.63	Co(II)	One	[37]
Alginate/Chitosan	3.18	Co(II)	One	[38]
Alginate/Chitosan	8.38	Cu(II)	One	[38]
Alginate/Chitosan	6.63	Cd(II)	One	[38]
Calcium alginate	97.08	Yi(III)	One	[39]
Alginate/COOH-CNTs	6.01	U(II)	One	[40]
Alginate-chitosan/COOH-CNTs	383	Co(II)	Six times	This work

in subsequent adsorption six times. This behavior is due to promising properties of functional groups (functional groups of CNTs and the polymeric matrix), porosity, the interaction between components, and size of nanoparticles. The presence of COOH-MWCNTs in the polyelectrolytic complex and insoluble nature of the Algi+Chito matrix provided reactive centers and stability to nanocomposites with variable voids and channels. The  $\text{Co}^{2+}$  ions can react physico-chemically with the sorbents by either adsorbing into voids or reacting with functional groups. Thus, the research outcome was that prepared adsorbents performed better than other alginate-based sorbents by adsorbing  $\text{Co}^{2+}$  ions pollutants. This better performance of sorbents also proved its economic importance since it is economical for industrial uses. The present research strongly recommends the use of synthesized sorbents in the industry for water purifying purposes.

#### 4. Conclusion

This study focused on the monitoring and removal of Co(II) ions from the aqueous solution by using novel alginate-chitosan/CNTs sorbents. The adsorbents were physically and chemically characterized, and adsorption parameters were systematically studied to know the maximum capturing capacity at optimum experimental conditions. The synthesized materials showed encouraging results in removing the Co(II) ions due to unique features like high stability, surface area, and coordinating reactive centers. Sorbents showed maximum adsorption capacities (381, 380, and 383  $\text{mg g}^{-1}$  for Cs90, Cc90, and CD90 films) at optimized conditions (400 ppm, 3 h, 7 pH, and 25°C). Moreover, the adsorption of Co(II) ions on prepared sorbents followed the pseudo-second-order kinetics, Freundlich nonlinear, and Langmuir linear isotherm models. Both the separation factor ( $R_L$ ) and Chi-square ( $\chi^2$ ) values claimed the suitability of the Langmuir model over the Freundlich model in adsorption of Co(II) ions having a monolayer nature. Thermodynamic study of adsorption of Co(II) was also carried out and found to be a favorable reaction with  $\Delta G^\circ$  values were  $-515.927$ ,  $-511.15$ , and  $-530.10$   $\text{kJ mol}^{-1}$ , respectively for Cs90, Cc90, and CD90 samples. The presence of different competing ions like K(I), Ca(II), Fe(III), Zn(II), Cu(II), and Ni(II) interfered with Co(II) ions to adsorb and non-selective nature of the film was obtained to adsorb other kinds of pollutants. Prepared samples have the potential to reuse in several cycles without affecting their performance in comparison with other alginate-based sorbents. Thus, the present study suggests the feasibility of alginate-chitosan/CNTs nanomaterials be used as low-cost adsorbents for the removal of heavy metal ions.

#### Acknowledgments

The authors are thankful to Dr. Muhammad Imran Shehzad (NCP Pakistan) and Mr. Bilal Akram Tsinghua University China for help in characterizing the samples.

#### References

- [1] M.J. Ascott, D.C. Gooddy, D.J. Lapworth, M.E. Stuart, Estimating the leakage contribution of phosphate dosed drinking water to environmental phosphorus pollution at the national-scale, *Sci. Total Environ.*, 572 (2016) 1534–1542.
- [2] F. Karkeh-Abadi, S. Saber-Samandari, S. Saber-Samandari, The impact of functionalized CNT in the network of sodium alginate-based nanocomposite beads on the removal of Co(II) ions from aqueous solutions, *J. Hazard. Mater.*, 312 (2016) 224–233.
- [3] S.W. Zhang, Z.Q. Guo, J.Z. Xu, H.H. Niu, Z.S. Chen, J.Z. Xu, Effect of environmental conditions on the sorption of radiocobalt from aqueous solution to treated eggshell as biosorbent, *J. Radioanal. Nucl. Chem.*, 28 (2011) 121–130.
- [4] Chemical Properties of Cobalt – Health Effects of Cobalt – Environmental Effects of Cobalt, LENNTECH. Available at: <https://www.lenntech.com/periodic/elements/co.htm>
- [5] X.W. Tang, Z.Z. Li, Y.M. Chen, Adsorption behavior of Zn(II) on calcinated Chinese Loess, *J. Hazard. Mater.*, 161 (2009) 824–834.
- [6] H. Aylin Devrimci, A. Mete Yuksel, F. Dilek Sanin, Algal alginate: a potential coagulant for drinking water treatment, *Desalination*, 299 (2012) 16–21.
- [7] M.T. Yagub, T.K. Sen, S. Afroze, H.M. Ang, Dye and its removal from aqueous solution by adsorption: a review, *Adv. Colloid Interface Sci.*, 209 (2014) 172–184.
- [8] Y.S. Ho, G.A. McKay, A comparison of chemisorption kinetic models applied to pollutant removal on various sorbents, *Process Saf. Environ. Prot.*, 76 (2009) 332–340.
- [9] M.R. Awual, M.M. Hasan, A. Islam, A.M. Asiri, M.M. Rahman, Optimization of an innovative composited material for effective monitoring and removal of cobalt(II) from wastewater, *J. Mol. Liq.*, 298 (2020) 112035, doi: 10.1016/j.molliq.2019.112035.
- [10] M.R. Awual, A. Islam, M.M. Hasan, M.M. Rahman, A.M. Asiri, M.A. Khaleque, M.C. Sheikh, Introducing an alternate conjugated material for enhanced lead(II) capturing from wastewater, *J. Cleaner Prod.*, 224 (2019a) 920–929.
- [11] J. Li, S. Zhang, C. Chen, G. Zhao, X. Yang, J. Li, X. Wang, Removal of Cu(II) and fulvic acid by graphene oxide nanosheets decorated with  $\text{Fe}_3\text{O}_4$  nanoparticles, *ACS Appl. Mater. Interfaces.*, 4 (2012) 4991–5000.
- [12] J. Abdi, M. Vossoughi, N. Mohammad Mahmoody, I. Alemzadeh, Synthesis of metalorganic framework hybrid nanocomposites based on GO and CNT with high adsorption capacity for dye removal, *Chem. Eng. J.*, 326 (2017) 1145–1158.
- [13] A. Nasrullah, A.H. Bhat, A. Naeem, M.H. Isa, M. Danish, High surface area mesoporous activated carbon-alginate beads for efficient removal of methylene blue, *Int. J. Biol. Macromol.*, 107 (2018) 1792–1799.
- [14] F. Aziz, M. El Achaby, A. Lissaneddine, K. Aziz, N. Ouazzani, R. Mamouni, L. Mandi, Composites with alginate beads: a novel design of nano-adsorbents impregnation for large-scale continuous flow wastewater treatment pilots, *Saudi J. Biol. Sci.*, 37 (2020) 2499–2508.
- [15] K. Norajit, K.M. Kim, G.H. Ryu, Comparative studies on the characterization and antioxidant properties of biodegradable alginate films containing ginseng extract, *J. Food Eng.*, 98 (2010) 377–384.
- [16] L. Zhu, L. Zhang, Y. Tang, D. Ma, J. Yang, Synthesis of kaolin/sodium alginate-grafted poly(acrylic acid-co-2-acrylamido-2-methyl-1-propane sulfonic acid) hydrogel composite and its sorption of lead, cadmium, and zinc ions, *J. Elastomers Plast.*, 47 (2015) 488–501.
- [17] B. Wang, Y. Wan, Y. Zheng, X. Lee, T. Liu, Z. Yu, J. Huang, Y.S. Ok, J. Chen, B. Gao, Alginate-based composites for environmental applications: a critical review, *Crit. Rev. Env. Sci. Technol.*, 49 (2019) 318–356.
- [18] M.A. Kamal, S. Bibi, S.W. Bokhari, A.H. Siddique, T. Yasin, Synthesis and adsorptive characteristics of novel chitosan/graphene oxide nanocomposite for dye uptake, *React. Funct. Polym.*, 110 (2017) 21–29.
- [19] S. Thakur, S. Pandey, O.A. Arotiba, Development of a sodium alginate-based organic/inorganic superabsorbent composite hydrogel for adsorption of methylene blue, *Carbohydr. Polym.*, 153 (2016) 34–46.
- [20] M. Kawaguchi, T. Fukushima, T. Hayakawa, N. Nakashima, Y. Inoue, S. Takeda, K. Okamura, K. Taniguchi, Preparation

- of carbon nanotube-alginate nanocomposite gel for tissue engineering, *Dent. Mater. J.*, 25 (2006) 719–725.
- [21] M.S. Islam, M. Ashaduzzaman, S.M. Masum, J.H. Yeum, Mechanical and electrical properties: electrospun alginate/carbon nanotube composite nanofiber, *Dhaka Univ. J. Sci.*, 60 (2012) 125–128.
- [22] Y. Zhuang, F. Yu, H. Chen, J. Zheng, J. Ma, J. Chen, Alginate/graphene double-network nanocomposite hydrogel beads with low swelling, enhanced mechanical properties, and enhanced adsorption capacity, *J. Mater. Chem. A*, 4 (2016) 10885–10892.
- [23] A.M. Alsharabasy, S.A. Moghannem, W.N. El-Mazny, Physical preparation of alginate/chitosan polyelectrolyte complexes for biomedical applications, *J. Biomater. Appl.*, 30 (2015) 1071–1079.
- [24] A. Bibi, Sadiq-ur Rehman, R. Faiz, T. Akhtar, M. Nawaz, S. Bibi, Effect of surfactants on swelling capacity and kinetics of alginate-chitosan/CNTs hydrogel, *Mater. Res. Exp.*, 6 (2019) 085065.
- [25] H. Lee, Y.C. Bae, Effect of surfactants on the swelling behaviors of thermosensitive hydrogels: applicability of the generalized Langmuir isotherm, *RSC Adv.*, 6 (2016) 103811–103821.
- [26] M.R. Awual, Efficient phosphate removal from water for controlling eutrophication using novel composite adsorbent, *J. Cleaner Prod.*, 228 (2019b) 1311–1319.
- [27] L. Pavia, G.M. Lampman, G.S. Kriz, *Introduction to Spectroscopy: A Guide for Students of Organic Chemistry*, W.B. Saunders Co., Philadelphia, 1979.
- [28] Y. Ou, C.H. Zhang, S.D. Li, L. Yang, J.J. Dong, X.L. Mo, Thermal degradation kinetics of chitosan-cobalt complex as studied by thermogravimetric analysis, *Carbohydr. Polym.*, 82 (2010) 1284–1289.
- [29] S.C.M. Fernandes, C.S.R. Freire, A.J.D. Silvestre, N.C. Pascoal, A. Gandini, L.A. Berglund, L. Salmen, Transparent chitosan films reinforced with a high content of nano-fibrillated cellulose, *Carbohydr. Polym.*, 8 (2010) 394–401.
- [30] D. Kulig, A. Zimoch-Korzycka, A. Jarmoluk, K. Marycz, Study on alginate-chitosan complex formed with different polymers ratio, *Polymers*, 8 (2016) 167, doi: 10.3390/polym8050167.
- [31] S.G. Muntean, M.A. Nistor, E. Muntean, A. Todea, R. Ianoş, C. Păcurariu, Removal of colored organic pollutants from wastewaters by magnetite/carbon nanocomposites: single and binary systems, *J. Chem.*, 2018 (2018) 1–16, doi: 10.1155/2018/6249821.
- [32] R. Fiaz, M. Hafeez, R. Mahmood, *Ficus palmata* leaves as a low-cost biosorbent for methylene blue: thermodynamic and kinetic studies, *Water Environ. Res.*, 91 (2019) 689–699.
- [33] A. Hassan, A. Abdel-Mohsen, M.M. Fouda, Comparative study of calcium alginate, activated carbon, and their composite beads on methylene blue adsorption, *Carbohydr. Polym.*, 102 (2014) 192–198.
- [34] M. Hamzaoui, B. Bestani, N. Benderdouche, The use of linear and nonlinear methods for adsorption isotherm optimization of basic green 4-dye onto sawdust-based activated carbon, *J. Mater. Environ. Sci.*, 9 (2018) 1110–1118.
- [35] X. Yang, T. Zhou, B. Ren, A. Hursthouse, Y. Zhang, Removal of Mn(II) by sodium alginate/graphene oxide composite double-network hydrogel beads from aqueous solutions, *Sci. Rep.*, 8 (2018) 1–16.
- [36] C. Jiao, J. Xiong, J. Tao, S. Xu, D. Zhang, H. Lin, Y. Chen, Sodium alginate/graphene oxide aerogel with enhanced strength-toughness and its heavy metal adsorption study, *Int. J. Biol. Macromol.*, 83 (2016) 133–141.
- [37] W. Jung, B.H. Jeon, D.W. Cho, H.S. Roh, Y. Cho, S.J. Kim, D.S. Lee, Sorptive removal of heavy metals with nano-sized carbon immobilized alginate beads, *J. Ind. Eng. Chem.*, 26 (2015) 364–369.
- [38] T. Gotoh, K. Matsushima, K.I. Kikuchi, Preparation of alginate-chitosan hybrid gel beads and adsorption of divalent metal ions, *Chemosphere*, 55 (2004) 135–140.
- [39] M. Khotimchenko, V. Kovalev, E. Khozhaenko, R. Khotimchenko, Removal of yttrium(III) ions from water solutions by alginate compounds, *Int. J. Sci. Environ. Technol.*, 12 (2015) 3107–3116.
- [40] H. Allaboun, M.M. Fares, F.A. Abu Al-Rub, Removal of uranium and associated contaminants from aqueous solutions using functional carbon nanotubes-sodium alginate conjugates, *Minerals*, 6 (2016) 9, doi: 10.3390/min6010009.